

## Predicted rotation signatures in MHD disc winds and comparison to DG Tau observations

N. Pesenti<sup>1</sup>, C. Dougados<sup>1</sup>, S. Cabrit<sup>2</sup>, J. Ferreira<sup>1</sup>, F. Casse<sup>3</sup>, P. Garcia<sup>4</sup>, and D. O'Brien<sup>4</sup>

<sup>1</sup> Laboratoire d'Astrophysique, UMR 5571, Observatoire de Grenoble, BP 53, 38041 Grenoble Cedex 9, France

<sup>2</sup> LERMA, UMR 8112, Observatoire de Paris, 61 avenue de l'Observatoire, 75014 Paris, France

<sup>3</sup> Institute for Plasma Physics Rijnhuizen, PO Box 1207, 3430 BE Nieuwegein, The Netherlands

<sup>4</sup> Centro de Astrofísica da Universidade do Porto, Rua das Estrelas, 4150-762 Porto, Portugal

Received 6 October 2003 / Accepted 28 January 2004

**Abstract.** Motivated by the first detections of rotation signatures in the DG Tau jet (Bacciotti et al. 2002), we examine possible biases affecting the relation between detected rotation signatures and true azimuthal velocity for self-similar MHD disc winds, taking into account projection, convolution as well as excitation gradients effects. We find that computed velocity shifts are systematically smaller than the true underlying rotation curve. When outer slower streamlines dominate the emission, we predict observed shifts increasing with transverse distance to the jet axis, opposite to the true rotation profile. Determination of the full transverse rotation profile thus requires high angular resolution observations ( $<5$  AU) on an object with dominant inner faster streamlines. Comparison of our predictions with HST/STIS observations of DG Tau clearly shows that self-similar, *warm* MHD disc wind models with  $\lambda = 13$  and an outer radius of the disc  $\approx 3$  AU are able to reproduce detected velocity shifts, while *cold* disc wind models ( $\lambda > 50$ ) are ruled out for the medium-velocity component in the DG Tau jet.

**Key words.** ISM: jets and outflow – stars: formation – ISM: individual objects: DG Tau

### 1. Introduction

It is now widely accepted that a large scale magnetic field is responsible for both the acceleration and collimation of jets around young accreting stars. However, the exact launching zone (stellar surface, disc truncation radius or wide range of disc radii) remains subject to debate. So far, studies aimed at constraining proposed ejection models have concentrated on the jet collimation, poloidal velocities, and excitation conditions (Dougados et al. 2000; Lavalley-Fouquet et al. 2000; Bacciotti et al. 2000; Woitas et al. 2002).

The detection of rotation signatures in the DG Tau jet has recently opened new prospects to constrain MHD ejection models (Bacciotti et al. 2002). In particular, approximate launching radii  $\approx 0.3$ – $3$  AU were inferred in DG Tau, indicative of a disc wind (Anderson et al. 2003). In this Letter, we investigate two classes of self-similar disc wind models (Sect. 2) and analyse in detail the biases introduced in their observed rotation signatures by projection, beam dilution and emissivity gradients within the jet (Sect. 3). Implications for a proper interpretation of the DG Tau observations are discussed in Sect. 4.

### 2. Disc wind models

We concentrate our study on two classes of steady, self-similar MHD keplerian accretion discs driving jets. They are mainly characterized by 3 nondimensional free parameters (see Cabrit et al. 1999):  $\epsilon = h/R_0 \approx 0.1$ , where  $h$  is the disc scale height at the disc radius  $R_0$ ,  $\alpha_m \approx 1$ , related to the magnetic diffusivity parameter, and  $\xi \equiv d(\log \dot{M}_{acc})/d(\log R)$ , which controls the mass loading onto field lines. In these solutions,  $\xi$  is related to the magnetic lever arm  $\lambda \approx (R_A/R_0)^2$  ( $R_A$  is the cylindrical radius at the Alfvén surface) by the relation  $\lambda = 1 + 1/(2\xi)$  (Casse & Ferreira 2000a) and therefore  $\lambda$  does not vary with  $R_0$ . Ferreira (1997) obtained *cold* solutions powered by the Lorentz force only, i.e. where enthalpy is negligible (resulting in typical  $\lambda$  values  $\approx 50$ ). Detailed comparison with recent observations showed that these solutions reproduce the collimation properties of T Tauri microjets (Dougados et al. 2000), but give excessive terminal poloidal velocities (Garcia et al. 2001b). More recently, Casse & Ferreira (2000b) computed *warm* disc wind solutions where entropy is injected at the flow base allowing for larger mass loads ( $\lambda \approx 10$ ) hence lower asymptotic velocities. In the following, we adopt a *cold* solution with  $\lambda = 50$  and a *warm* solution with  $\lambda = 13$ . Dimensional scaling parameters are set as follows: the inner and outer radii of the disc involved in the ejection process are  $R_i = 0.07$  AU (typical corotation radius for a T Tauri star) and

Send offprint requests to: N. Pesenti,  
e-mail: Nicolas.Pesenti@obs.ujf-grenoble.fr

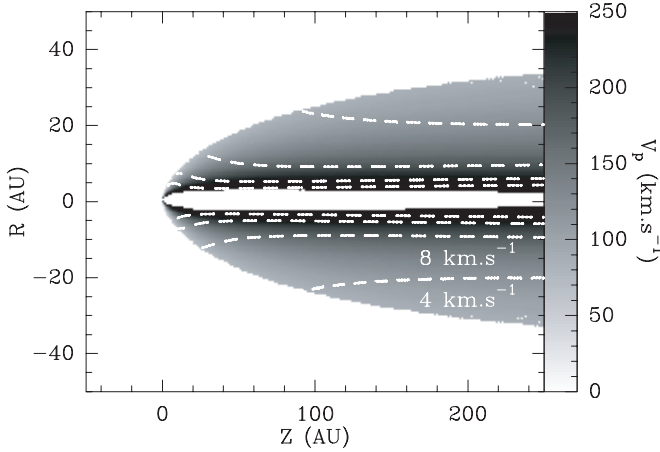


**Fig. 1.** Velocity components ( $V_p, V_\phi$ ) in the ( $R, Z$ ) plane for the *warm* solution ( $\lambda = 13$ ). Dashed lines:  $V_\phi$  varying from 4 to 16  $\text{km s}^{-1}$  by steps of 4  $\text{km s}^{-1}$ . Greyscale:  $V_p$ .

$R_e = 1$  AU (where molecules are supposed to start to form), the accretion rate through the disc  $\dot{M}_{\text{acc}} = 10^{-6} M_\odot \text{yr}^{-1}$  and the central stellar mass  $M_\star = 0.5 M_\odot$ . The ejection efficiency ( $2 \dot{M}_{\text{jet}}/\dot{M}_{\text{acc}} = \xi \times \ln R_e/R_i$ ) is then 3% for the *cold* solution and 10% for the *warm* one.

Asymptotic toroidal velocities in MHD disc winds depend mainly on the magnetic lever arm  $\lambda$  and  $R_0$ . In Fig. 1, we show poloidal and toroidal velocities in the ( $R, Z$ ) plane for the *warm* solution. The *cold* solution shows a similar map with predicted toroidal and poloidal velocities larger by a factor 2. For a given streamline,  $V_\phi$  rapidly decreases with distance  $Z$  along the jet until the maximum expansion radius is reached (at  $Z/R = 25$  and 20 for the *cold* and *warm* solutions respectively).

To calculate predicted rotation signatures for the above models, we constructed synthetic long-slit spectra perpendicular to the jet axis (transverse PV diagrams) and convolved them by a two-dimensional Gaussian beam to simulate the instrumental spatial and spectral resolutions. The effect of rotation is to induce a “tilt” in transverse PV diagrams (dashed lines, Fig. 2a). We then get a synthetic velocity shift  $V_{\text{shift}}$  by cross-correlating extracted velocity spectra at symmetric positions with respect to the jet axis (Figs. 2b,c). Our computations show that  $V_{\text{shift}}$  values are only weakly dependent on the adopted spectral resolution, provided line profiles are well sampled. We will use here the a velocity resolution of  $50 \text{ km s}^{-1}$ , which is accessible to current imaging spectrographs, and smaller than line profile widths. We adopt a typical inclination of  $i = 45^\circ$  with respect to the line of sight (Pyo et al. 2003) and consider transverse PV diagrams at  $Z_{\text{proj}} = 50\text{--}60$  AU.

We will use the [O I]  $\lambda 6300$  line, the effect of a tracer with lower critical density being discussed later. We explore spatial resolution effects by varying the beam size ( $FWHM$ ) between 1 AU and 14 AU. To calculate line emissivities in the *cold* solution, we use the thermal and ionization structure computed a posteriori by Garcia et al. (2001a) with ambipolar diffusion heating. The resulting  $T_e$  is roughly constant ( $T_e \sim 10^4$  K) and the ionization stratification is close to a  $x_e \propto 1/R_0$  law. This gives line profiles with a strong high velocity component (HVC), originating from the inner faster streamlines

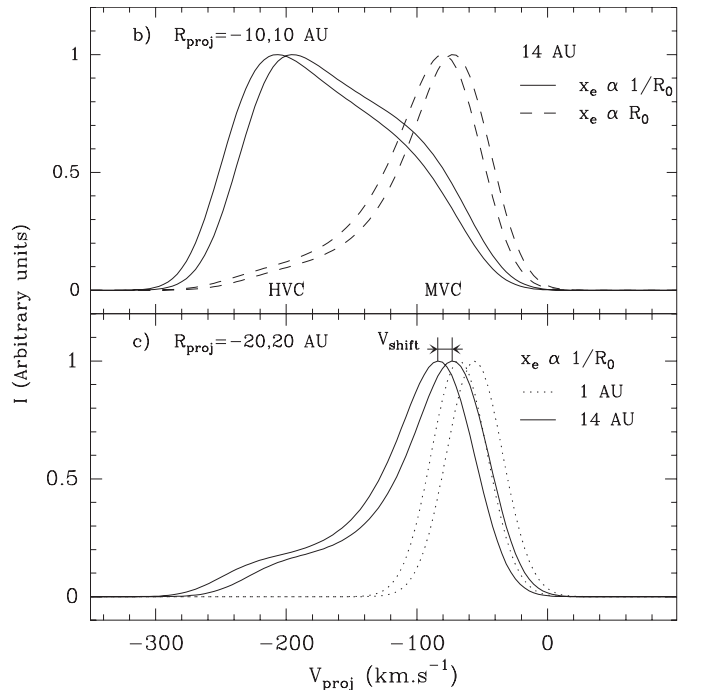
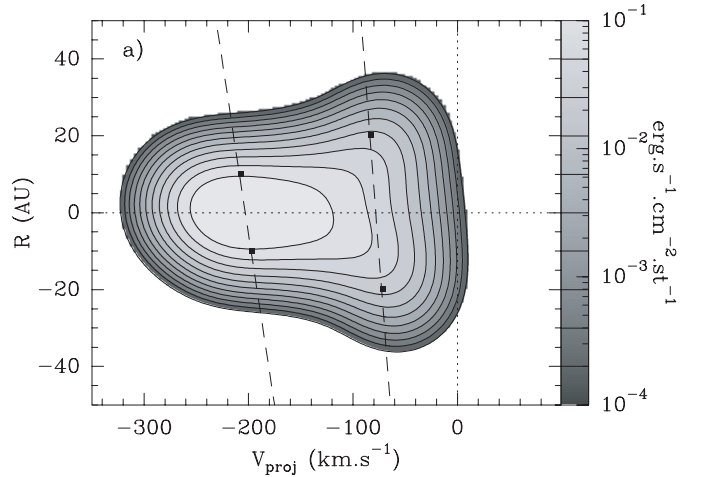


**Fig. 2. a)** Synthetic transverse Position-Velocity (PV) diagram for the *warm* solution (integrated over  $Z_{\text{proj}} = 50\text{--}60$  AU) in the [O I]  $\lambda 6300$  line, convolved with a 14 AU  $\times 50 \text{ km s}^{-1}$  beam.  $i = 45^\circ$  and  $x_e = 0.1 \times (0.1 \text{ AU}/R_0)$ . Dashed lines are indicative of peak velocity shifts at 10 and 20 AU from the jet axis. **b)** Velocity profiles extracted from PV diagrams at  $R_{\text{proj}} = \pm 10$  AU, convolved with a spatial beam of 14 AU for  $x_e = 0.1 \times (0.1 \text{ AU}/R_0)$  (solid lines) and  $x_e = 0.1 \times (R_0/1 \text{ AU})$  (dashed lines), **c)** and at  $R_{\text{proj}} = \pm 20$  AU, with spatial beams of 1 (dotted) and 14 AU (solid) for  $x_e = 0.1 \times (0.1 \text{ AU}/R_0)$ .

(Garcia et al. 2001b). In the case of the *warm* solution, where the full thermal solution is not yet available, we keep  $T_e = 10^4$  K and we explore two extreme ionization fraction laws: one similar to the *cold* solution,  $x_e = 0.1 \times (0.1 \text{ AU}/R_0)$ , where the HVC dominates (solid curves in Fig. 2b), and one with  $x_e = 0.1 \times (R_0/1 \text{ AU})$ , where emission from outer slower streamlines is enhanced, and the profile is dominated by a medium velocity component (MVC, dashed curves, Fig. 2b). The latter case reproduces better observed line profiles in the

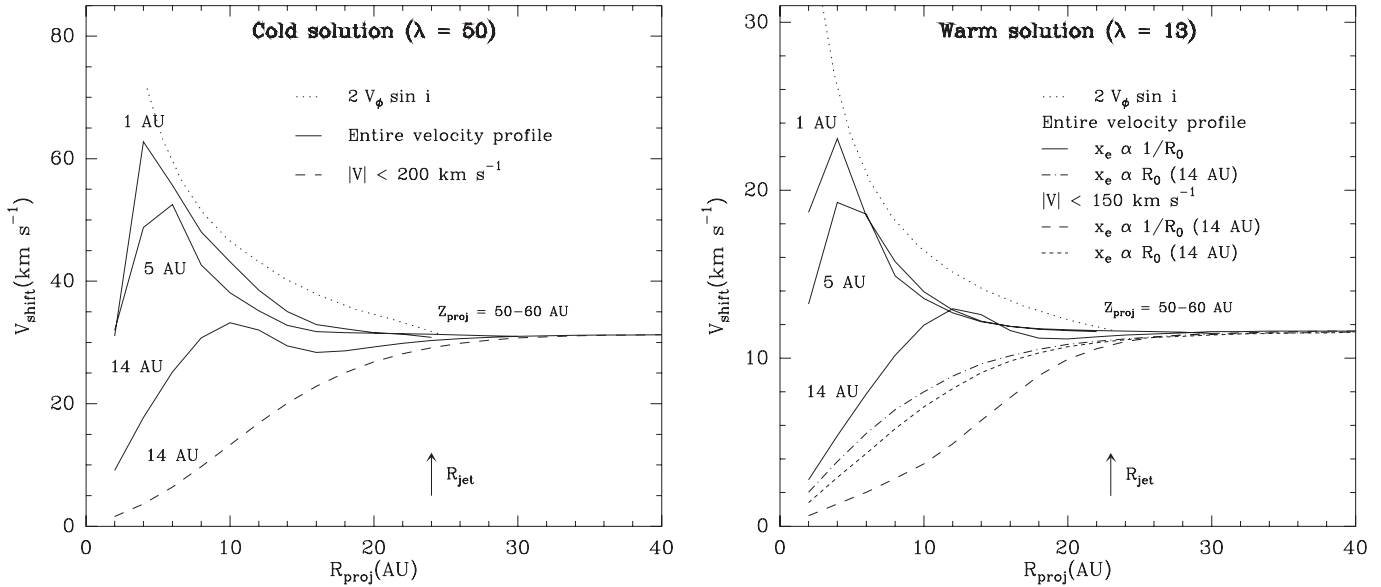


**Fig. 3.** Velocity shifts predicted by the disc wind models as a function of projected transverse radius  $R_{\text{proj}}$ . *Left:* cold solution with the thermal structure of Garcia et al. (2001a). *Right:* warm solution with two ionization fraction laws (see Sect. 2 for more details).  $V_{\text{shift}}$  are obtained by cross-correlating [O I]  $\lambda 6300$  line profiles at  $\pm R_{\text{proj}}$ , extracted from a transverse PV diagram at  $Z_{\text{proj}} = 50\text{--}60$  AU. Solid and dash-dotted lines:  $V_{\text{shift}}$  computed using the entire velocity profile, short-dashed and long-dashed lines: or restricting to the MVC. Dotted lines show the projected underlying true azimuthal profile extracted from the corresponding wind solution.  $R_{\text{jet}}$  is the outermost jet radius (for  $R_e = 1$  AU).

DG Tau jet (see Bacciotti et al. 2002), and allows us to investigate the effect of various emissivity gradients in the jet on the observed  $V_{\text{shift}}$ .

### 3. Detailed analysis of disc wind predictions

We first discuss  $V_{\text{shift}}$  values obtained by cross-correlation over the entire velocity profile, plotted in Fig. 3. We also plot for comparison as a dotted curve the projected azimuthal velocity profile ( $V_{\text{shift}}^{\text{theo}}(R) = 2 \times V_{\phi}(R) \times \sin i$ ) extracted from the corresponding wind solution at the same  $Z_{\text{proj}}$ . We find that measured velocity shifts always underestimate the true rotation profile, especially at small transverse distances from the jet axis. This underestimate comes from the integration of the flow along the line of sight, combined with projection effects: at a given radius  $R_{\text{proj}}$  from the jet axis, the line of sight intersects a range of flow surfaces with true cylindrical radii  $R > R_{\text{proj}}$ . Due to the Keplerian law, they rotate more slowly than  $V_{\phi}(R_{\text{proj}})$ . In addition, these outer surfaces are not tangent to the line of sight and their projected rotation speed is  $\sin i \times V_{\phi}(R) \times \sin \phi$  with  $\sin \phi = R_{\text{proj}}/R$  introducing an additional reduction factor. However, the exact amount by which the rotation profile is underestimated by these projection effects critically depends on excitation gradients and beam dilution, as we now discuss.

We first consider the case where inner streamlines (HVC) dominate line profiles, which is illustrated by the cold solution and the warm solution with  $x_e \propto 1/R_0$  (solid curves, Fig. 3). A given beam tends to decrease  $V_{\text{shift}}$  at projected radii below the beam diameter (see 14 AU beam, Fig. 3) because of cancellation effects between opposite sides of the jet. When  $R_{\text{proj}}$  varies from the beam diameter to the jet outer radius  $R_{\text{jet}}$ , each profile is dominated by the surface at  $R = R_{\text{proj}}$  and the discrepancy from the theoretical value is small. Only at radii smaller than

the central hole radius  $R_{\text{hole}}$  (4 AU for both solutions),  $V_{\text{shift}}$  tend to zero as  $R_{\text{proj}}/R_{\text{hole}}$ , due to the above projection effect.

We examine now the case where outer streamlines (MVC) dominate line profiles, which is illustrated by the warm solution with  $x_e \propto R_0$  (dash-dotted curves, Fig. 3). Line profiles at  $R_{\text{proj}}$  are now strongly contaminated by surfaces with true radii  $R > R_{\text{proj}}$ , so that  $V_{\text{shift}}$  lies significantly below  $V_{\text{shift}}^{\text{theo}}$  (a factor 2 at 10 AU), regardless of beam size. Only  $V_{\text{shift}}$  measured at projected distances on the order of  $R_{\text{jet}}$  fit correctly  $V_{\text{shift}}^{\text{theo}}$ , the projection factor  $R_{\text{proj}}/R$  being then  $\sim 1$ .

Finally, when cross correlation is made on the MVC only (long-dashed and short-dashed curves, Fig. 3),  $V_{\text{shift}}$  is even lower and varies almost as  $R_{\text{proj}}/R_{\text{jet}}$ . This can be understood by considering that cross-correlation on the MVC is sensitive only to a narrow range of outer streamlines at  $R \sim R_{\text{jet}}$ . Beam smearing and excitation gradients have little effect because this region is far from the jet axis and has roughly homogeneous excitation conditions.

We have verified that the above results remain valid over a broad region of the parameter space. Variation of  $M_{\star}$ ,  $R_i$  and  $R_e$  only introduces scaling factors ( $V \propto \sqrt{M_{\star}/R_0}$ ),  $R_{\text{hole}}$  and  $R_{\text{jet}}$  being about proportional to  $R_i$  and  $R_e$  respectively.  $V_{\text{shift}}$  obtained from a solution with  $\lambda = 8$  have the same biases as those described above, suggesting that our results also do not depend critically on the detailed disc wind model. The only other parameter of significant influence on the predicted  $V_{\text{shift}}$  is the electronic density to critical density ratio ( $N_e/N_{\text{cr}} = N_{\text{H}}x_e/N_{\text{cr}}$  with  $N_{\text{H}}$ , the total density) for a given line. If  $N_e/N_{\text{cr}} > 1$  in the central parts of the jet, either because the accretion rate is increased ( $\dot{M}_{\text{acc}} \propto N_{\text{H}}$ ) or a tracer with low  $N_{\text{cr}}$  (such as [S II]  $\lambda 6731$ ) is used, the emissivity saturates and  $V_{\text{shift}}$  becomes significantly lower than  $V_{\text{shift}}^{\text{theo}}$  (though not as much as for MVC-dominated profiles). A ratio  $N_e/N_{\text{cr}} < 1$  in the inner part

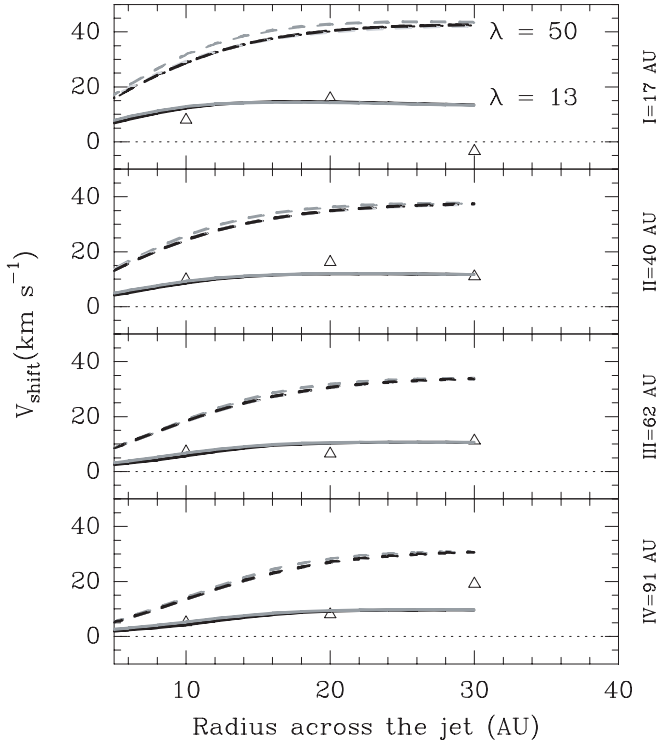


**Fig. 4.** Velocity shifts as a function of radius at four deprojected distances from the star, 17 to 91 AU, obtained by cross-correlation over the MVC. Symbols: DG Tau observations (Bacciotti et al. 2002). Curves: predictions for the *cold* (dashed;  $R_e = 1$  AU) and *warm* (solid;  $R_e = 3$  AU) disc wind solutions in [S II]  $\lambda 6731$  (light grey), [O I]  $\lambda 6300$  (dark grey) and [Fe II]  $\lambda 644 \mu\text{m}$  (black), computed with the estimated inclination angle of DG Tau jet ( $45^\circ$ ; Pyo et al. 2003) and with the beam size of HST/STIS ( $0.1'' \times 50 \text{ km s}^{-1}$ ).

of the jet, and thus a tracer with high  $N_{\text{cr}}$ , is needed to retrieve the shape of  $V_{\text{shift}}$  curves shown in Fig. 3 in the HVC-dominated case for high accretion rates.

#### 4. Comparison with DG Tau observations

We compare here our predictions with observations of DG Tau carried out by Bacciotti et al. (2002) with HST/STIS.  $V_{\text{shift}}$  were obtained from the MVC by cross-correlation techniques similar to the one described in Sect. 2. In Fig. 4, we plot observed  $V_{\text{shift}}$  (symbols) and predictions for both disc wind models with an equivalent beam size ( $0.1'' \times 50 \text{ km s}^{-1}$ ) and at the same distances (deprojected) from the star. Predicted velocity shifts are plotted in several spectral lines, and are seen to differ by less than 10%.

We first note that both the *cold* and *warm* solutions reproduce well the trend of increased measured  $V_{\text{shift}}$  with transverse radius in DG Tau. Based on the above study, we interpret this trend as due to projection effects only. Thus, measurements at  $R_{\text{proj}} = 10, 20 \text{ AU} < R_{\text{jet}}(Z)$  do not yield direct measures of  $V_\phi$ , but only lower limits. Only data points at  $R_{\text{proj}} = 30 \text{ AU}$ , close to the outer jet radius, would be expected to give true  $V_\phi$ .

Second, we note that  $V_{\text{shift}}$  deduced from the *cold* disc wind model  $\approx 30\text{--}40 \text{ km s}^{-1}$  are about by a factor 3–6 too high compared to observed velocity shifts of  $6\text{--}15 \text{ km s}^{-1}$ . Steady, self-similar *cold* solutions with lower toroidal velocities (lower  $\lambda$ ) exist, but terminate too close to the star ( $Z/R_0 \leq 10$ ; Ferreira 1997). This class of solutions is therefore definitely excluded for the MVC in the DG Tau jet. On the other hand, the *warm* disc wind solution with  $\lambda = 13$  fit very well observed  $V_{\text{shift}}$  in the DG Tau jet within instrumental uncertainties, except for the 30 AU datapoints in region I and IV. Far from the jet axis, region I suffer from a poor signal-to-noise ratio, while region IV may be contaminated by non-axisymmetric structures in the external medium and/or bowshocks, similar to those at larger scale (Lavalley-Fouquet et al. 2000).

Although the difference in  $V_{\text{shift}}$  between  $R_e = 1$  and 3 AU is less than 25%, we note that the latter  $R_e$  value is essential for reproducing observed centroid velocities  $\approx 50 \text{ km s}^{-1}$  of the MVC in DG Tau ( $\approx 80 \text{ km s}^{-1}$  would be found for  $R_e = 1 \text{ AU}$ ; see Fig. 2b). This value is consistent with results of the diagnostic method of disc wind launching radii proposed by Anderson et al. (2003). However, launching radii  $R_0 = 0.3\text{--}1 \text{ AU}$  deduced with this method from the underestimated azimuthal velocities at  $R_{\text{proj}} = 10, 20 \text{ AU}$ , are only lower limits. Observations with a spatial beam  $< 5 \text{ AU}$  and high-density tracers for ionized gas, favouring HVC-dominated line profiles, would allow to derive the full transverse velocity profile ( $\propto 1/\sqrt{R}$ ), and also more constraints on  $\lambda$ ,  $R_i$  and  $R_e$ . Such a resolution is currently achievable in the UV domain with HST/STIS and in the near-IR domain with the new generation of adaptive optics system operating on 8 m class telescopes such as NACO on the VLT.

*Acknowledgements.* We would like to thank the referee, F. Bacciotti, for her very helpful comments.

#### References

- Anderson, J. M., Li, Z., Krasnopolsky, R., & Blandford, R. D. 2003, *ApJ*, 590, L107
- Bacciotti, F., Mundt, R., Ray, T. P., et al. 2000, *ApJ*, 537, L49
- Bacciotti, F., Ray, T. P., Mundt, R., Eisloffel, J., & Solf, J. 2002, *ApJ*, 576, 222
- Cabrit, S., Ferreira, J., & Raga, A. C. 1999, *A&A*, 343, L61
- Casse, F., & Ferreira, J. 2000, *A&A*, 353, 1115
- Casse, F., & Ferreira, J. 2000, *A&A*, 361, 1178
- Dougados, C., Cabrit, S., Lavalley, C., & Ménard, F. 2000, *A&A*, 357, L61
- Ferreira, J. 1997, *A&A*, 319, 340
- Garcia, P. J. V., Ferreira, J., Cabrit, S., & Binette, L. 2001a, *A&A*, 377, 589
- Garcia, P. J. V., Cabrit, S., Ferreira, J., & Binette, L. 2001b, *A&A*, 377, 609
- Lavalley-Fouquet, C., Cabrit, S., & Dougados, C. 2000, *A&A*, 356, L41
- Pyo, T.-S., Kobayashi, N., Hayashi, M., et al. 2003, *ApJ*, 590, 340
- Woitas, J., Ray, T. P., Bacciotti, F., Davis, C. J., & Eisloffel, J. 2002, *ApJ*, 580, 336